geosciences

MDPI

Article

Variable Response in Alpine Tree-Ring Stable Isotopes Following Volcanic Eruptions in the Tropics and Iceland

Tito Arosio [1,2,3,*], Stéphane Affolter [4], Kurt Nicolussi [5], Michael Sigl [1,2], Malin Michelle Ziehmer-Wenz [1,2,6], Christian Schlüchter [2,7], Emmanuel Schaad [1,2], Rafael Stähli [1,2] and Markus Christian Leuenberger [1,2,*]

1 Climate and Environmental Physics, Physics Institute, University of Bern, 3012 Bern, Switzerland
2 Oeschger Centre for Climate Change Research, University of Bern, 3012 Bern, Switzerland
3 Department of Geography, University of Cambridge, Cambridge CB2 3EN, UK
4 Quaternary Geology, Department of Environmental Sciences, University of Basel, 4056 Basel, Switzerland
5 Institute of Geography, University of Innsbruck, 6020 Innsbruck, Austria
6 Swiss Tropical and Public Health Institute, 4051 Basel, Switzerland
7 Institute of Geological Sciences, University of Bern, 3012 Bern, Switzerland
* Correspondence: ta530@cam.ac.uk (T.A.); markus.leuenberger@unibe.ch (M.C.L.)

Abstract: The importance of the stable isotopes in tree rings for the study of the climate variations caused by volcanic eruptions is still unclear. We studied $\delta^{18}O$, δD, $\delta^{13}C$ stable isotopes of larch and cembran pine cellulose around four major eruptions with annual resolution, along with a superposed epoch analysis of 34 eruptions with 5-year resolution. Initial analysis of the tropical Tambora (1815 CE) and Samalas (1257 CE) eruptions showed a post-eruption decrease in $\delta^{18}O$ values attributed to post-volcanic cooling and increased summer precipitation in Southern Europe, as documented by observations and climate simulations. The post-volcanic cooling was captured by the δD of speleothem fluid inclusion. The $\delta^{18}O$ decrease was also observed in the analysis of 34 major tropical eruptions over the last 2000 years. In contrast, the eruptions of c. 750, 756, and 764 CE attributed to Icelandic volcanoes left no significant responses in the cellulose isotopes. Further analysis of all major Icelandic eruptions in the last 2000 years showed no consistent isotopic fingerprints, with the exception of lower post-volcanic $\delta^{13}C$ values in larch. In summary, the $\delta^{18}O$ values of cellulose can provide relevant information on climatic and hydroclimatic variations following major tropical volcanic eruptions, even when using the 5-year resolution wood samples of the Alpine Tree-Ring Isotope Record database.

Keywords: volcanic eruption; tree rings; stable isotope; fluid inclusion; Alps; climate

Citation: Arosio, T.; Affolter, S.; Nicolussi, K.; Sigl, M.; Ziehmer-Wenz, M.M.; Schlüchter, C.; Schaad, E.; Stähli, R.; Leuenberger, M.C. Variable Response in Alpine Tree-Ring Stable Isotopes Following Volcanic Eruptions in the Tropics and Iceland. *Geosciences* **2022**, *12*, 371. https://doi.org/10.3390/geosciences12100371

Academic Editors: Marcello Liotta and Jesus Martinez-Frias

Received: 5 August 2022
Accepted: 5 October 2022
Published: 8 October 2022

1. Introduction

Major volcanic eruptions are important drivers of short-term climate variability [1]. Such eruptions can cause surface cooling on regional and global scales through stratospheric injection of aerosols and fine ash particles [2]. The solid ash particles have a residence time of a few months, but the volcanic gases—especially SO_2 and H_2S—produce much more significant effects, as they reach global coverage in the troposphere and form sulphuric acid (H_2SO_4) aerosols with a residence time of 1–3 years [1]. Aerosols backscatter incoming solar radiation, resulting in net cooling at the surface [1]. The climatic impacts are affected by the geographical location and other source parameters of the eruptions. Those at low latitudes often produce global aerosol dispersion, whereas those in high-latitude areas, such as Iceland, typically disperse aerosols only in the hemisphere where they are located [3,4]. The global climatic impacts of some volcanic eruptions have left evident historical and environmental records, including the explosive eruptions of Tambora in 1815 CE [5] and Krakatau in 1883 CE [6] in Indonesia, as well as the long-lasting fissure eruption of Laki in 1783/84 [7,8] in Iceland. These eruptions had effects on the global and regional temperatures, and they could also have effects on the hydrological cycle, changing

the amounts of summer precipitation [9,10]. The post-eruption spring and summer cooling is a homogeneous response that occurs both regionally and globally [11–14], while the hydroclimatic response is much more spatially heterogeneous [15].

Tree rings are among the few paleoclimate proxies that provide continuous annual resolution [16] with high dating accuracy [17]. This makes them very important for dating and studying past eruptions [2,18]. Trees are living organisms, and environmental changes affect their metabolism, producing changes that are recorded in the biomass growth rate, which is detectable in tree-ring parameters [16]. Tree-ring width (TRW) has mainly been used as indicator of plant growth, which depends on various limiting factors—predominantly on temperature and water availability [16]. Therefore, TRW has been used to date some eruptions [19–21] and to study their climatic impact [22–24]. However, TRW can overestimate the duration of volcanic cooling, since the strong climatic variation caused by the eruptions can have a long-lasting effect on the tree growth [25,26]. This does not occur for another tree-ring proxy—the maximum latewood density (MXD), which exhibits a minor memory effect [27]. Stable isotopes of the tree rings' cellulose ($\delta^{13}C$, $\delta^{18}O$, and δD) have been used to complement the climatic information gained from TRW [28], but only a few studies have examined how they respond to volcanic eruptions, e.g., [24,29–31]. These studies indicated variability of the responses depending on the isotope, tree type, and location. For example, eco-physiological responses of $\delta^{13}C$ and $\delta^{18}O$ in European trees were reported following eruptions of volcanoes located at mid-latitudes [32] or at high latitudes [30]. Other volcanic eruptions imprinted signals in the $\delta^{13}C$ and $\delta^{18}O$ values of trees grown at high latitudes or high altitudes [31], as well as those of oaks in Central Europe [33]. The isotope values of Southern European oaks were sensitive to summer drought and showed a decade-long dry trend after 12 Icelandic eruptions [33]. However, they did not record tropical eruptions [33], while the TRWs of pines from different sites in the Northern Hemisphere were temperature-sensitive and showed post-eruption cold signals [34]. A multi-tree-ring study on volcanic eruptions showed a site-specific climate influence on Siberian larch, but with a general decrease in carbon and oxygen isotope ratios in the first five years after the eruption, along with a long-lasting sequence of small tree-ring width in the post-eruption period, reflecting changes in temperature and sunshine duration [31].

The conifers growing at high altitudes in the Alps are among the best trees to study to analyse the climatic response following volcanic eruptions. They are particularly sensitive to summer temperature, precipitation, and sunshine duration, and their cellulose $\delta^{18}O$ values have been shown to be influenced by large-scale synoptic circulation, with a strong common signal of different sites and species [35]. Moreover, their $\delta^{13}C$ values reflect local climatic conditions with species-specific signals [36,37] and can be linked to temperature and precipitation [35,38,39]. In contrast, their δD values have not been widely used for climate interpretation, as they contain strong biological signals that have not been fully elucidated [40,41].

Additionally, the hydrogen isotope composition of fluid inclusion of speleothems (hereafter δD_{fi}) records past climate variability—particularly temperature variability [42]. It integrates climate information over the whole year, including the cold season, complementing the tree-ring proxies that are sensitive to the warm season. It has already been suggested to be sensitive to the climatic effects of volcanic eruptions [42]. However, it is characterised by a greater age uncertainty compared to tree rings, which achieve single-year precision [42,43].

The present work discusses variability of stable isotopes in the cellulose of the tree-ring samples of the past 2000 years in the Alpine Holocene Triple Tree-Ring Isotope Record project (AHTTRIR) [44]. It aims to verify how they were affected by the climate fluctuations following major volcanic eruptions over the last two millennia, and to compare them to deuterium in the fluid inclusion of speleothems to better understand the short-term climatic signals.

Initially, we investigated single eruption events, studying the periods around major eruptions of the tropics (e.g., 1809 and Tambora 1815 CE) and others attributed to Iceland (i.e., in 750, 756, and 764 CE, with an absolute age uncertainty of ± 1 year) at annual time resolution, along with other major eruptions (e.g., Samalas 1257 or Laki 1783) at 5-year time resolution. Then, we investigated 34 major eruptions of the last 2000 years via a superposed epoch analysis approach [2] to detect a general volcanic fingerprint on

the cellulose isotopes. Additionally, the stable isotope data were compared with other published tree-ring proxies—tree-ring width (TRW) and maximum density (MXD)—and with an independent proxy, i.e., the paleotemperatures based on the hydrogen isotope composition of speleothem fluid inclusion water from Milandre Cave in Switzerland.

2. Materials and Methods

2.1. Subfossil Wood Samples and Sampling Sites in the Alps

The wood sections were made available by the Department of Geography of the University of Innsbruck, where the Eastern Alpine Conifer Chronology (EACC) was compiled based on a calendar-dated tree-ring width series [43]. The samples were from deciduous larch (*Larix decidua Mill.*) and the evergreen cembran pine (*Pinus cembra* L.). They were collected from treeline sites in different parts of the European Alps covering a southwest–northeast transect with an elevation range between 1930 and 2400 m (Figure 1). The wood samples continuously cover the past 9000 years, and only a few of them contain tree rings that grew after the Industrial Revolution, i.e., after 1850 CE. The tree-ring width of all samples was measured with a precision of ±0.001 mm, as described in [43]. Dated tree samples with relatively wide rings were selected in order to collect enough material for the isotope measurements. As described in previous studies [45,46] and in the publicly available database AHTTRIR [44], all of the wood samples of the database have a 5-year resolution, and they were prepared and analysed for stable oxygen, carbon, and hydrogen isotope ratios. The same procedure was used to resolve annual rings of four trees—two larches and two cembran pines—by precisely cutting annual rings for the time intervals between 1800 and 1825 CE and between 720 and 780 CE.

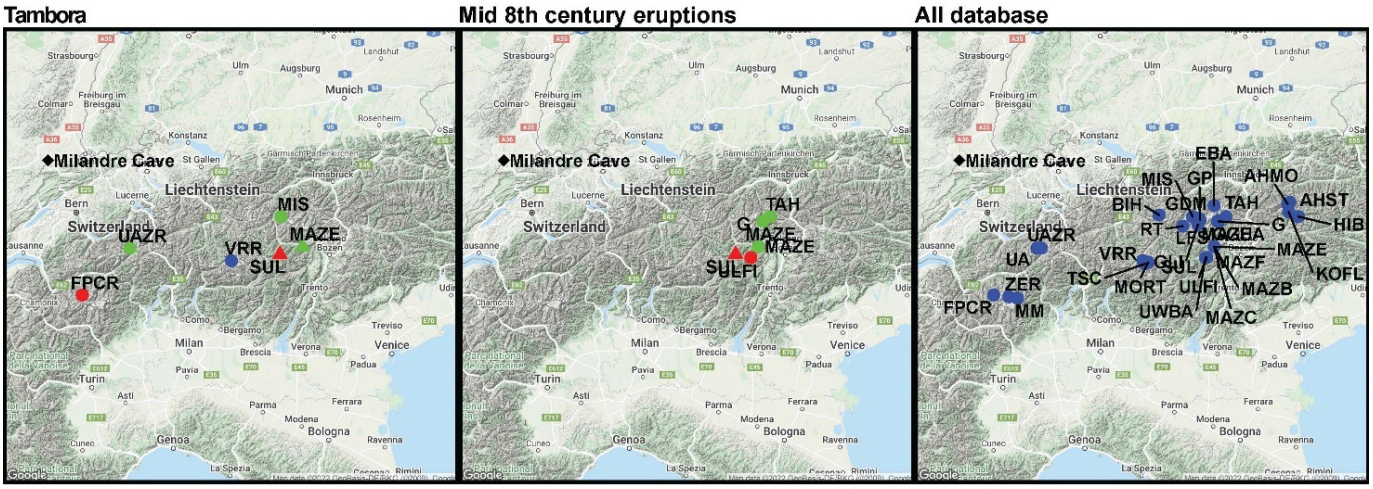

Figure 1. Sampling locations of the analysed tree and speleothem samples: Green symbols correspond to sites where cembran pines were collected, red symbols indicate larch samples, and blue symbols denote where samples of both species were collected. Dots indicate the sites of isotope samples with 5-year resolution, while triangles represent the sites of annually resolved isotope series. The black rhomboid corresponds to Milandre Cave, from which the speleothem record originates. **Left** panel: sampling sites of the trees covering the Tambora eruption. **Central** panel: location of the trees covering the mid-8th-century Icelandic eruptions; the site MAZE provides samples with both resolutions. **Right** panel: all sites of the Eastern Alpine Conifer Chronology (EACC) that provided material for the complete tree-ring isotope dataset: green = cembran pine, red = larch samples, and blue = both species.

2.2. Stable Isotope Analysis and Carbon Isotope Correction

The cellulose extraction procedure, the determination of the cellulose content [46], and the $\delta^{13}C$, δD, and $\delta^{18}O$ isotope analysis [47] have been described previously. Briefly, we used continuous-flow isotope-ratio mass spectrometry (Isoprime 100) coupled with a

pyrolysis unit (HEKAtech GmbH, Wegberg, Germany) similar to the Thermo Scientific high-temperature conversion elemental analyser (TC/EA; for technical details see [47]). This approach was extended to measure the exchangeable hydrogen of alpha-cellulose using the online equilibration method [47,48]. The results are reported in parts per thousand (‰) relative to the Vienna Pee Dee Belemnite (VPDB) for carbon and to the Vienna Standard Mean Ocean Water (VSMOW) for hydrogen and oxygen [49]. The precision of the measurement was ±3.0 ‰ for hydrogen, ±0.3 ‰ for oxygen, and ±0.15 ‰ for carbon [47]. Time series of the isotope results are given in Figure 2. The "Alpine Holocene Triple Tree Ring Isotope Record" (AHTTRIR) database used in this work is now publicly accessible [44].

Fossil fuel burning and land-use changes in the Industrial Revolution from about 1850 onward led to a continuous increase in atmospheric carbon dioxide (CO_2), which is depleted in $\delta^{13}C$ [50]—known as the Suess effect [51]. This change is reflected in the carbohydrates of the plants; therefore, a correction must be made to the isotopic series of the tree rings. For all of the $\delta^{13}C$ values after 1000 CE, we applied the correction factor described previously [50].

2.3. Selected Major Volcanic Eruptions

The samples of the AHTTRIR database have a 5-year resolution, which might be too large for the short-term climatic variations that follow the eruptions. To verify this, we also analysed samples with annual resolution obtained from one cembran pine and one larch for the periods around 4 major eruptions: that of Tambora (1815), the preceding—yet unidentified—eruption [52,53] in 1809, and two mid-8th-century eruptions attributed to Icelandic volcanoes (750 and 764). Additionally, an Icelandic eruption (Laki, 1783–1784) and a tropical eruption (Samalas, 1257) were analysed at the 5-year resolution only. We analysed the tropical and the non-tropical eruptions separately; see Figure 1 for the corresponding sample locations. The eruption of Tambora (Indonesia) in April 1815 is an example of a tropical eruption.

Tambora had a major impact on the global climate, especially in Europe and North America (Supplementary Figure S1a). The released aerosols led to substantial annual cooling of the tropics and the extratropical Northern Hemisphere by approximately 0.4–0.8 °C compared to the preceding 30 years. Large socioeconomic impacts following widespread crop failures and subsequent famines in 1816 have been partially associated with the Tambora eruption [5,54]. The 1257 eruption of the tropical Samalas volcano in Indonesia [55] was one of the largest eruptions of the Common Era [56]. The sulphur deposits in ice cores were twice as large as those of the Tambora eruption in 1815 [2]. The years following the eruption—1258 and 1259—experienced some of the coldest Northern Hemisphere summers of the past millennium. However, cooling in the Northern Hemisphere was spatially heterogeneous [57,58].

An example of a non-tropical eruption is the 1783–1784 Laki eruption in Iceland (Grímsvötn volcano), which began on 8 June 1783 and lasted episodically for 8 months until February 1784. The eruption in the summer of 1783 is thought to have caused air temperatures in the Northern Hemisphere to drop by about 1.0 °C, and to have caused winter cooling over a period of three years after the eruption [7,59]. Unlike shortlived explosive eruptions such as Tambora (CE 1815) and Pinatubo (CE 1991), long-lasting high-latitude fissure eruptions such as Laki are not as well-understood in terms of their sulphate dispersal, radiative forcing, and atmospheric circulation. The persistence of Laki sulphate aerosols in the atmosphere and their effects on regional climate are also uncertain, as are the magnitude and duration of volcano-induced radiative forcing of climate and its impacts (Supplementary Figure S1b) [60].

In addition to Grímsvötn and Bárdarbunga, Katla volcano is also a source of large subglacial explosive eruptions of predominantly basaltic magmas in Iceland. With an average return interval of 50 years, Katla is Iceland's most active volcanic system [61]. Katla, Grímsvötn, and Bárdarbunga all had volcanic eruptions dated to the mid-8th century [62–65], and here we tentatively attribute a sequence of three volcanic sulphate peaks detected in Greenland ice cores dated to CE 750, 756, and 764 to Icelandic eruptions. We

note that [66] assumed eruption latitudes of 45° N (CE 750 and 756) and 0° (CE 764) in their reconstruction of stratospheric aerosol optical depth (SAOD) from ice-core records.

2.4. Superposed Epoch of the Major Volcanic Eruptions after 1 CE

We further investigated 34 different strong volcanic eruptions that occurred during the last 2000 years [2] (see Table S1). The eruption parameters for the 34 volcanic eruptions used in the superposed epoch analyses are based on the work of Toohey and Sigl [66]. We selected all eruptions with a global mean stratospheric aerosol optical depth (SAOD) $\geq$ SAOD of Krakatau (1883) and all eruptions with SAOD30-90° N > 0.10 (e.g., Veiðivötn 1477 CE, Katla 822 CE).

For each eruption, we chose a preceding background period without a known major eruption and compared the post-eruption isotopic signals (see Table S1). Only trees covering both periods were selected. We superimposed the data of the different eruptions by assigning 0 to the time (years) of each eruption. For each tree, we converted the values into anomalies from the mean of the period 15 to 5 years before the volcanic eruption. Since oxygen was the only isotope for which there was coherence among values between species [67] and the climate sensitivity was similar, we merged the values of two species for the oxygen isotope and kept the species separated for the carbon and hydrogen isotopes.

2.5. Relation of Cellulose Isotopes to Climatic Parameters

For this comparison, we used instrumental observation data of the HISTALP database [68] for temperature and precipitation—i.e., their anomalies from the 1800–2000 means—and for sunshine duration, i.e., its anomaly from the 1880–2000 mean, since the observational database for sunshine duration is shorter than those for temperature and precipitation. We calculated the 5-year averages of the anomalies to be compatible with the temporal resolution of the stable isotopes in cellulose. For the analyses, we created cellulose isotope mean series using the normalised values of individual trees to avoid some geographical or species effects. We applied Pearson's correlation between the time series for precipitation and temperature with the average series of each isotope type. The correlation was calculated from 1840 to 1970 CE for temperature and precipitation, and from 1880–1970 CE for sunshine duration.

3. Results

3.1. Early 19th Century Eruptions (of Tambora 1815 and Unidentified 1809 CE)

The stable isotopes of the period 1800–1825 CE were from wood specimens collected at the sites shown in Figure 1A. We studied tree rings with annual resolution from one larch and one cembran pine, as well as rings with 5-year resolution from two larches and four cembran pines. The solid lines in Figure 2 show the annual δD, $\delta^{18}O$, and $\delta^{13}C$ values of the period 1800–1825 for larch (LADE) and cembran pine (PICE). Variations in annual oxygen isotope values (Figure 2b) were similar for both species, with a minimum around 1815 followed by a continuous increase until 1820, but with larch showing additional minima in 1811 and 1812. The two larch trees with 5-year resolution (dotted lines) showed a similar pattern, with a decrease until 1815 followed by a steady increase. The four cembran pines with 5-year resolution also showed similar patterns, all with a steady decline until 1815, followed by an increase.

The annually resolved hydrogen isotope curve of cembran pine was consistent with the corresponding 5-year resolution curve—both were flat before the eruption date, followed by a general increase (Figure 2a). In contrast, for the larch there was a divergence between the annually resolved and 5-year resolution values, and they did not show consistent changes around the eruption.

The annually resolved values of the larch carbon isotope showed an evident increase in the period 1805–1815, followed by levelling off; a trend could be observed in one of the two trees with 5-year resolution (Figure 2c). In contrast, the annual values of cembran pine exhibited no trend and a negative peak centred on 1821, which was not visible in the four trees analysed with 5-year resolution. Consequently, $\delta^{13}C$ did not show consistent trends around this eruption.

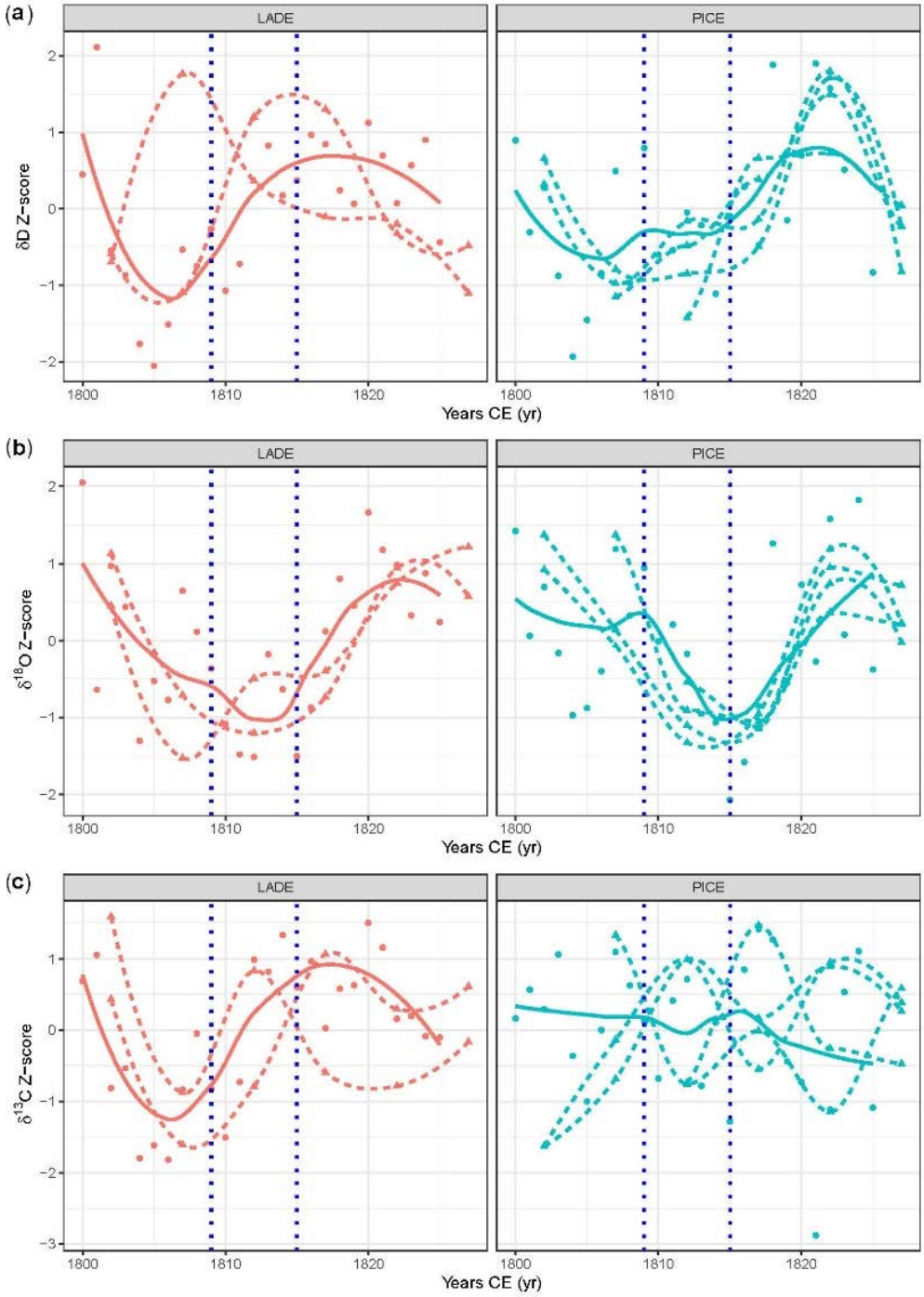

Figure 2. Plots of tree-ring cellulose isotopes for larch (LADE, red lines) and cembran pine (PICE, blue lines) at the time of the Tambora eruption; the points are the individual measurements, and the lines are the spline of each tree. Isotope series with annual resolution are shown with continuous lines, while the 5-year resolution series are given by dotted lines. The vertical dotted lines indicate the time of the Tambora eruption in 1815 CE and of an unidentified eruption occurring in 1809. Panel (**a**): δD values. Panel (**b**): $\delta^{18}O$ values. Panel (**c**): $\delta^{13}C$ values.

Furthermore, we performed a statistical analysis of the correlations between the different cellulose isotopes from 1800 to 1825 CE and between cembran pine and larch. The Pearson's correlation coefficient (r) between the annually resolved $\delta^{18}O$ values of the larch and cembran pine was 0.64 (p-value < 0.05). For δD, r was 0.53 (p-value = 0.05), while for $\delta^{13}C$ r was −0.07 and was non-significant (p-value > 0.05). The high correlation between

the oxygen isotope values of the two species allowed us to combine them in one chronology by averaging. However, this was not possible for the carbon isotope, as there was no correlation between larch and pine.

We then compared these results with the fluid-inclusion-based temperatures of a stalagmite from Milandre Cave in the Jura Mountains, which represent a mean annual or slightly cold season-biased temperature signal [42]. Despite their lower temporal resolution, they showed a cool phase followed by a positive post-eruption trend similar to Alpine conifer cellulose $\delta^{18}O$ records (Figure 3b). We also compared our cellulose $\delta^{18}O$ series with instrumental data and climate proxy records (Figure 3). These included the summer temperatures reconstructed from TRW data [69] (Figure 3e), temperatures reconstructed from MXD data [70] (Figure 3d), and instrumental annual mean temperatures from HISTALP measured in the Alps [68] (Figure 3c) and from the Swiss Plateau [71] (Figure 3f). A summary of the characteristics of the different records can be found in Table 1. The cellulose $\delta^{18}O$ record closely followed the HISTALP and MXD temperatures, with positive peaks in 1807 followed by a decline until 1815/16 and a subsequent increase until 1820. There was a temporal shift in the minimum around the Tambora eruption; in the cellulose $\delta^{18}O$ it occurred in 1815, while in the measured and reconstructed temperature records it occurred in 1816. The values of speleothem δD_{fi} showed a marked cool phase followed by an increase between 1815 and 1820. The TRW-based temperature reconstruction decreased until 1815, followed by a slightly negative trend until 1821, which was different from the other data.

Table 1. Comparison of our database with other paleoclimatic temperature reconstructions and temperature measurements.

	This Study	**This Study**	**Affolter et al. 2019**	**Büntgen et al. 2006**	**Büntgen et al. 2011**	**Auer et al. 2006**	**Climhist (Pfister, 2015)**
Proxy	δD, $\delta^{18}O$, $\delta^{13}C$ cellulose	δD, $\delta^{18}O$, $\delta^{13}C$ cellulose	δD fluid inclusion	MXD	TRW	HISTALP	Climhist Swiss Central Plateau temperature
Temporal resolution	Annual	5-Year	Multi-annual to Multi-decadal	Annual	Annual	Monthly	Monthly
Region	Alps	Alps	Europe	European Alps	Central Europe	European Alps	Swiss Central Plateau
Parameter			Temperature	Temperature	Temperature	Measured temperature	Measured temperature
Season			Annual	JJAS	JJA	JJA	All year
Periods	1800–1815 CE 750–780 CE	8930 b2k–2010 CE	−12596 BCE–2011 CE	755–2004 CE	499 BCE–2003 CE	1760–2008 CE	1760–2007

Pearson statistical analysis of the data from 1800 to 1825 CE showed significant correlation (p-value < 0.05) between the $\delta^{18}O$ of cellulose and (i) the temperature reconstruction from MXD (Figure 3d) (r = 0.66), (ii) the measured instrumental summer temperature values of HISTALP [68] (Figure 3c) (r = 0.48), and (iii) the temperature of the Swiss Plateau [71] (Figure 3f) (r = 0.41). In contrast, the correlation with the TRW-based temperature reconstruction was not significant (Figure 3e).

3.1.1. Mid-8th-century eruptions attributed to Iceland (750, 756, and 764 CE)

A series of eruptions attributed to Iceland occurred in the mid-8th century between 750 and 764 CE. The solid lines of Figure 4 show the annual $\delta^{18}O$, δD, and $\delta^{13}C$ values for the interval 720–780 CE for larch and cembran pine. The $\delta^{18}O$ records of both species (Figure 4b) show a good agreement between the annual and the 5-year resolution values, which remain within the variance range of the 25 years before the first eruption and show no changes around the years of the eruptions.

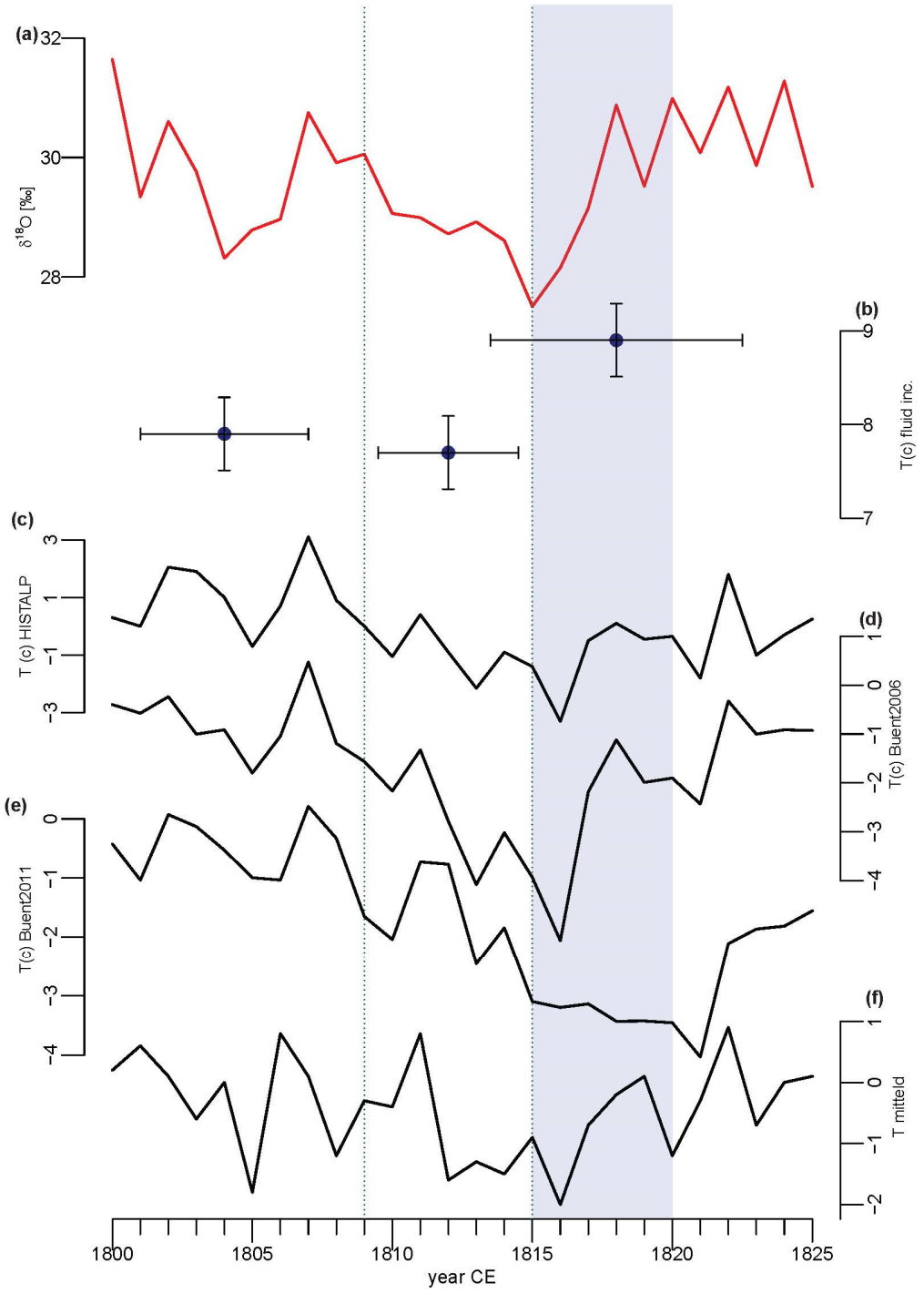

Figure 3. Comparison between the trends of tree-ring oxygen isotopes and those of other climate proxies in the period of the Tambora eruption: (**a**) Average series of the $\delta^{18}O$ values of the two trees with annual resolution. (**b**) Temperature from the speleothem fluid inclusions from Milandre Cave. (**c**) The summer temperature anomaly of instrumental climate observation from high-elevation sites of the HISTALP database. (**d**) Reconstructed summer temperature based on MDX by [70]. (**e**) Reconstructed temperature evolution based on TRW by [69]. (**f**) The annual temperature anomaly of the mean measured temperature on the Swiss Plateau [71].

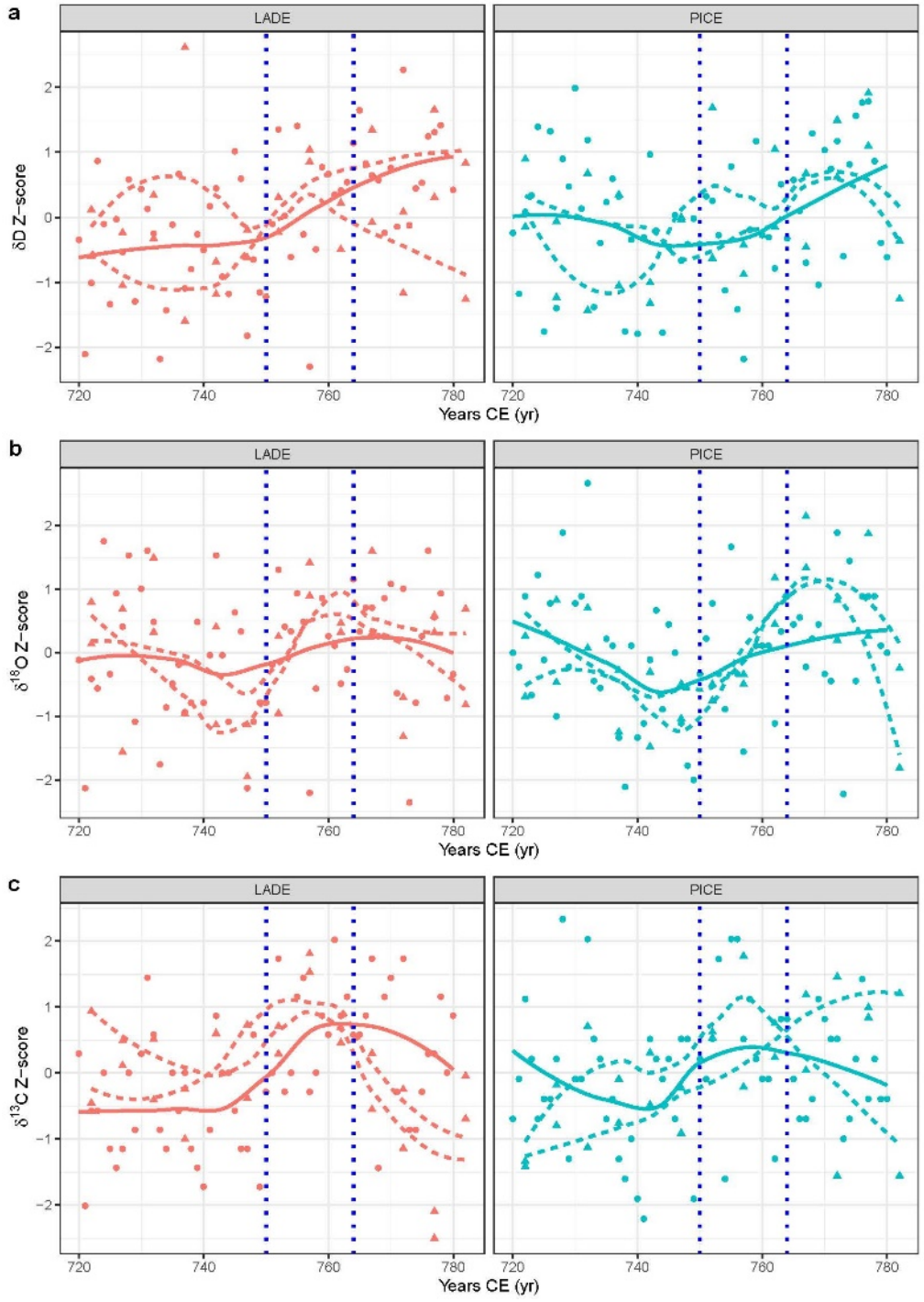

Figure 4. Plots of tree-ring cellulose isotope series in mid-8th-century eruptions attributed to Icelandic volcanoes; the points are the individual measurements, and the lines are the spline of each tree. The values of the series with annual resolution are shown by the continuous lines, while the values of the series with 5-year resolution are given by the dotted lines. The left column shows the values of larch samples (LADE, in red) and the right column shows the values of cembran pine (PICE, blue). The vertical dotted lines indicate the years of the eruptions (750 and 764 CE). Panel (**a**): δD values. Panel (**b**): $\delta^{18}O$ values. Panel (**c**): $\delta^{13}C$ values.

For the hydrogen isotope, the annual and 5-year resolution records overlap for both species (Figure 4a), except for the years 735 CE in larch and 750 CE in cembran pine. No significant

changes can be seen around the years of the three eruptions, i.e., the δD values remain within the variance interval of the 25 years before the first eruption, similar to the oxygen.

For the carbon isotope, the annual and 5-year resolution records also agree for both species (Figure 4c), with a minor exception for larch, where only the two 5-year-resolution trees have a negative peak at 765 CE. Thus, both species show higher values in the period between the first and last eruptions, but still within the range of variability of the time before the eruptions.

The Pearson's correlation coefficient (r) between the annually resolved $\delta^{18}O$ data for larch and cembran pine was 0.63; for δD it was 0.59, and it was 0.39 for $\delta^{13}C$; all of these correlations were significant. The high correlation for oxygen and hydrogen isotopes between the two species allowed them to be combined into average series, increasing the sample replication, as described above. The correlation coefficient (r) between the two mean series of hydrogen and oxygen isotopes was 0.73 and was significant. This averaging was not performed for the carbon isotope due to the low correlation value between the larch and cembran pine data.

Next, we compared the data of the cellulose isotopes with the speleothem fluid inclusion temperature values and the temperature reconstruction from TRW [69] (Figure 5). However, the time resolution of the speleothem samples was too low for this period. Lower values between 749 and 759 CE were found in the temperature reconstruction from TRW [69], while the cellulose $\delta^{18}O$ and δD values remained stable after the two eruptions.

3.1.2. Eruptions of Laki (1783–1784 CE) and Samalas (1257 CE)

The good agreement between the annual and 5-year resolution values of cellulose isotopes observed in the early 19th century and mid-8th century periods suggests that the large database of 5-year Alpine tree-ring isotope samples (AHTTRIR) can be used to study other major eruptions. We selected the Icelandic Laki eruption of 1783–1784 CE and the tropical Samalas eruption of 1257 CE as examples of high-latitude and tropical eruptions, respectively, since no other significant eruptions are known in the years around these events (Table S1). Figure 6 shows the plots of the cellulose isotopes of two larches and two cembran pines, the temperature reconstruction from speleothem fluid inclusion, and the temperature reconstructions from TRW and MXD for the period around the eruption of Laki. The $\delta^{18}O$ cellulose values of three out of the four trees show a positive peak in the year of the eruption (Figure 6a). These trees are from Engadin and Tyrol, while the tree without a peak is from the Valaisan Alps in Switzerland—differences that indicate regional sensitivity that may affect the records. The carbon (Figure 6b) and hydrogen isotope ratios (Figure 6c) show no evident trends around the eruption.

The temperature based on speleothem fluid inclusion shows a minimum close to the eruption time and an increase in values in the 10 years post-eruption (Figure 6d), while the temperature reconstruction from TRW displays a positive peak (Figure 6e), and the temperature reconstruction from MXD shows no evident signature around the eruption time (Figure 6f). Overall, the $\delta^{18}O$ of cellulose and calcite as well as the TRW-based temperature show positive peaks at the time of or after the eruption, but with different duration and absolute timing.

The climate proxy records for the period around the Samalas eruption are shown in Figure 7. The cellulose $\delta^{18}O$ values of two cembran pines show a negative peak at the time of the eruption (Figure 7a). The δD and $\delta^{13}C$ curves do not show evident patterns (Figure 7b,c). The speleothem record does not show any clear trend around the eruption time (Figure 7d), and the temperature reconstruction from MXD shows a negative post-eruption peak (Figure 7f). The temperature reconstruction from TRW shows no modification (Figure 7e). Overall, the data suggest that the 5-year AHTTRIR values can record the climate anomalies generated by some major eruptions, and that the geographic location of the eruptions may leave different imprints in the various stable isotope records.

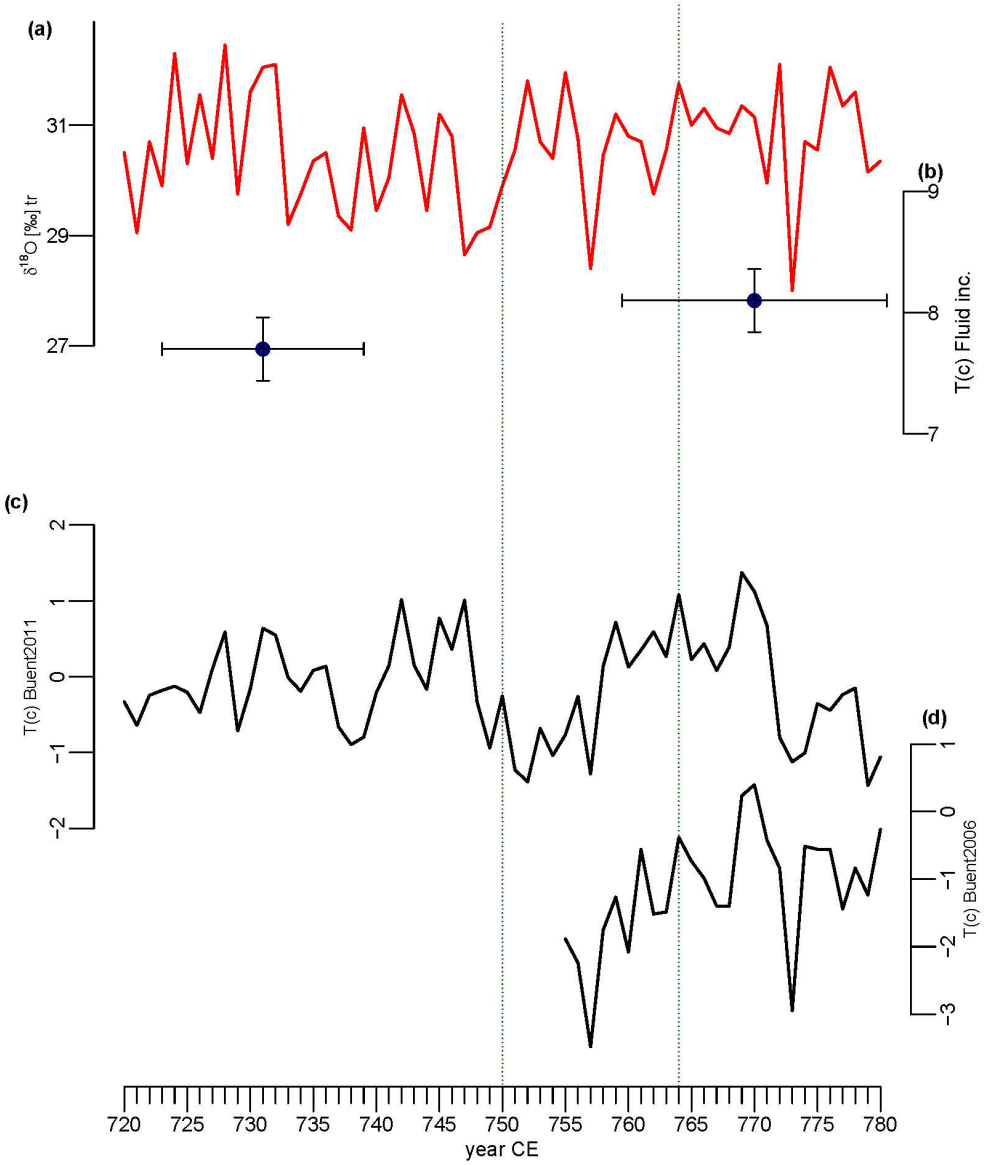

Figure 5. Comparison between the trend of the oxygen isotope series and those of other climate proxies in mid-8th-century eruptions attributed to Icelandic volcanoes: (**a**) Average series of the $\delta^{18}O$ values of the two trees with annual resolution. (**b**) Temperature from the speleothem fluid inclusions from Milandre Cave. (**c**) Reconstructed temperature evolution based on TRW by [69] (**d**) Reconstructed summer temperature based on MDX by [70].

3.1.3. Superposed Analysis of Large Volcanic Eruptions during the Past Two Millennia

We used the tree-ring isotope data with a 5-year resolution (AHTTRIR) to analyse the periods around 34 volcanic eruptions during the Common Era described in [2], including eruptions in both the extratropical Northern Hemisphere and the tropics. The data for each isotope for larch (red) and cembran pine (blue) are shown in Figure 8; we separated the values of the Northern Hemispheric Extratropical (NHET) and tropical eruptions from the Icelandic ones. We combined the values of the two species only for the oxygen isotope, as this signature is not species-specific, in contrast to the carbon and hydrogen isotopes [67].

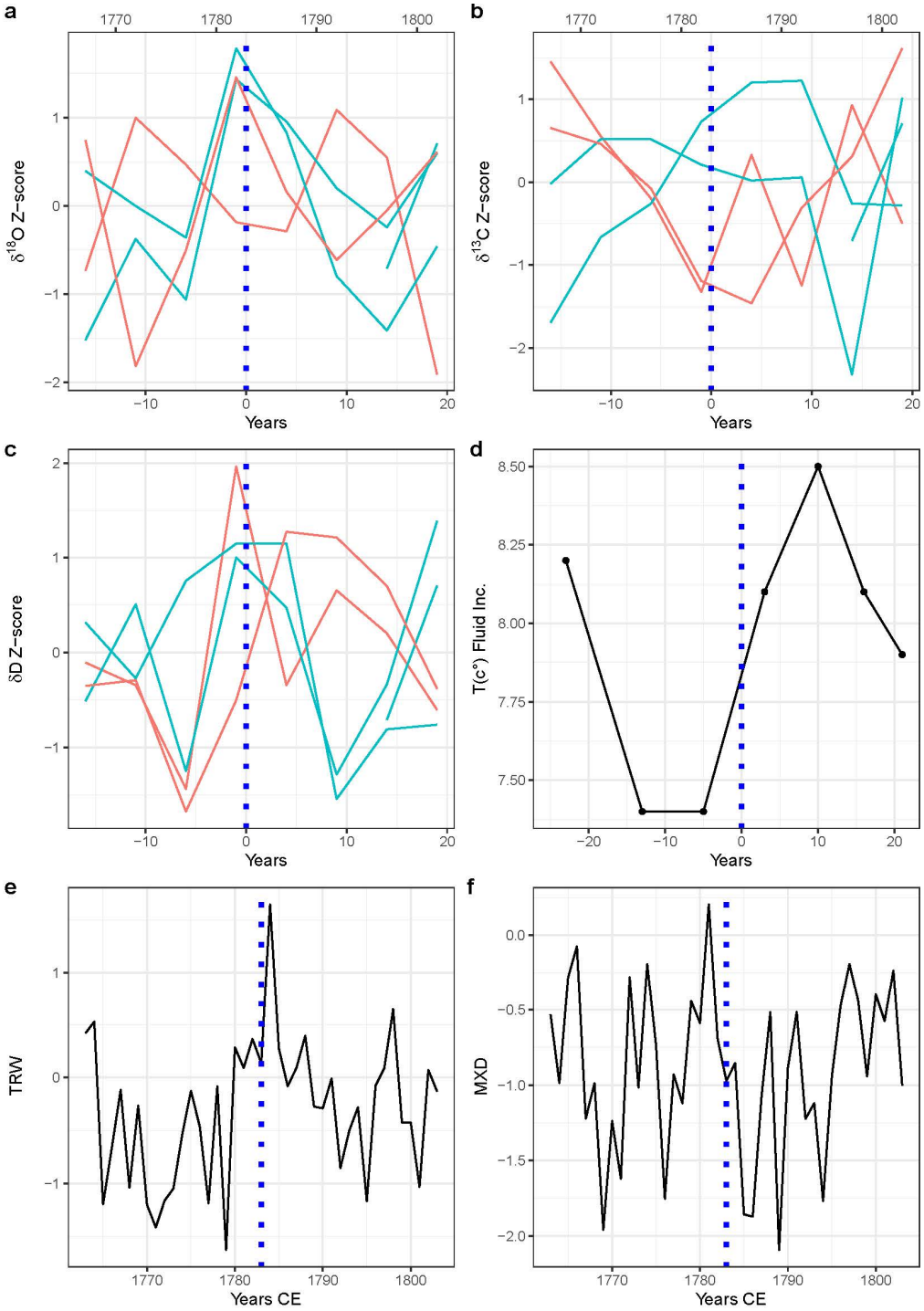

Figure 6. Plots of tree-ring cellulose isotopes and climate proxies in the period of the Laki eruption: (**a**) $\delta^{18}O$ of two larch trees (red) and of two cembran pines (blue) with 5-year resolution. (**b**) $\delta^{13}C$ of the trees above. (**c**) δD of the trees above. (**d**) Temperature reconstruction from fluid inclusions from Milandre Cave. (**e**) The temperature reconstruction based on TRW by Büntgen et al., 2011. (**f**) The temperature reconstruction based on MXD by Büntgen et al., 2006. The dotted vertical line indicates the eruption year (1783 CE).

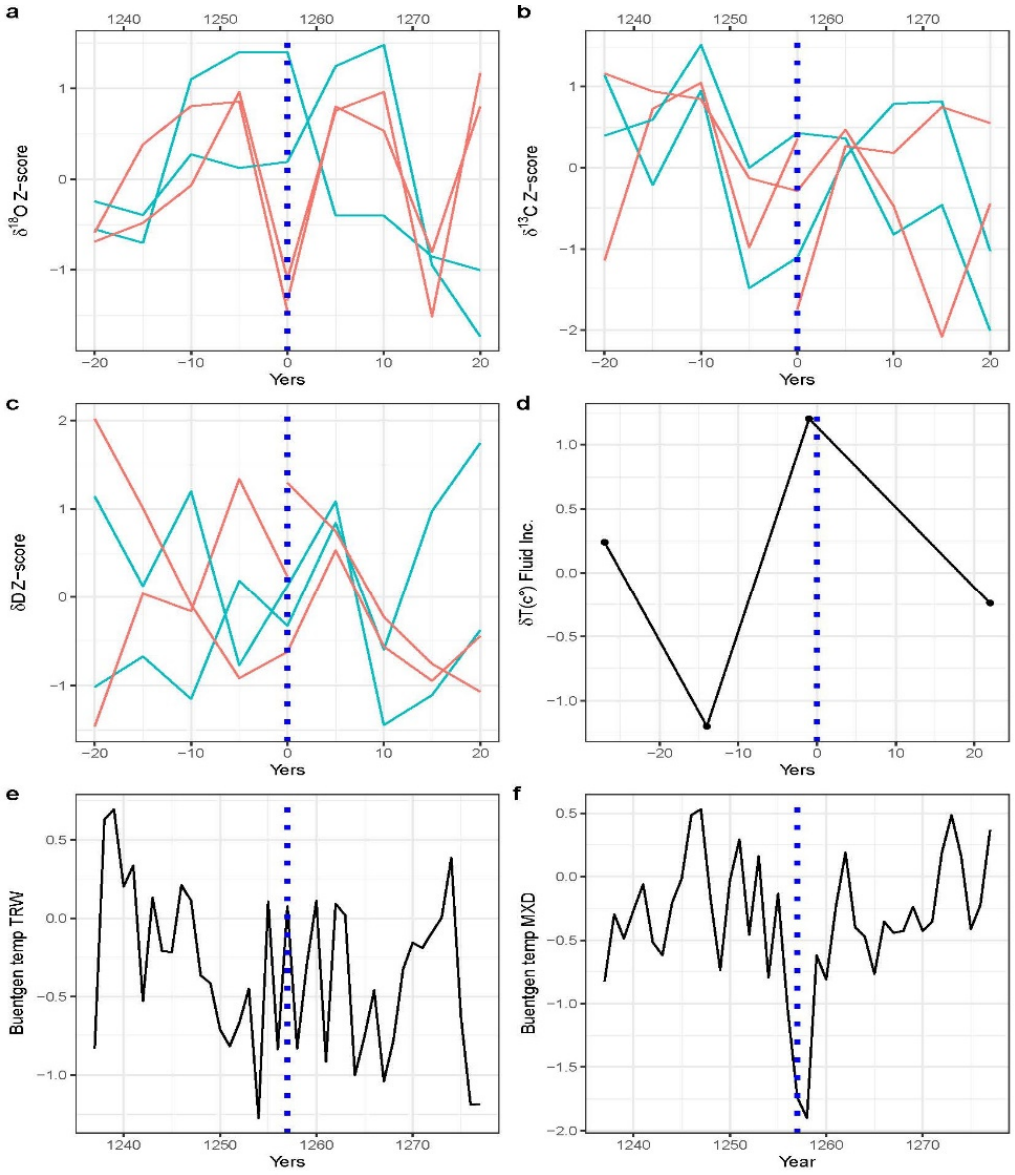

Figure 7. Plots of tree-ring cellulose isotopes and climate proxies in the period of the Samalas eruption, 1257 CE: (**a**) $\delta^{18}O$ of two larch trees (orange) and of two cembran pines (blue) with 5-year resolution; the dotted vertical line indicates the eruption year. (**b**) $\delta^{13}C$ of the trees from (**a**). (**c**) δD of the trees from (**a**). (**d**) Temperature reconstruction from fluid inclusions from Milandre Cave. (**e**) The temperature reconstruction based on TRW by Büntgen et al., 2011. (**f**) The temperature reconstruction based on MXD by Büntgen et al., 2006.

To compare and superpose the values of the 34 eruptions, the data around the eruptions were subtracted from the mean value of the pre-eruption period for each tree. The wood samples span 5-years, so that the time resolution is 5 years. The $\delta^{18}O$ data show a decrease around the "NHET + Tropical" eruptions with respect to the calibration period (Figure 8a). In contrast, the $\delta^{18}O$ values show no obvious changes after the Icelandic eruptions. The $\delta^{13}C$ values of cembran pine and larch values tended to reach more positive values up to 5 years after the "NHET + Tropical" eruptions, while they increased after the Icelandic eruptions (Figure 8b). There was a small increase in both species of deuterium around the Icelandic eruptions. Larch does not show a clear behaviour in "NHET + Tropical" eruptions, unlike cembran pine, which displays a lower value around "NHET + Tropical" eruptions (Figure 8c).

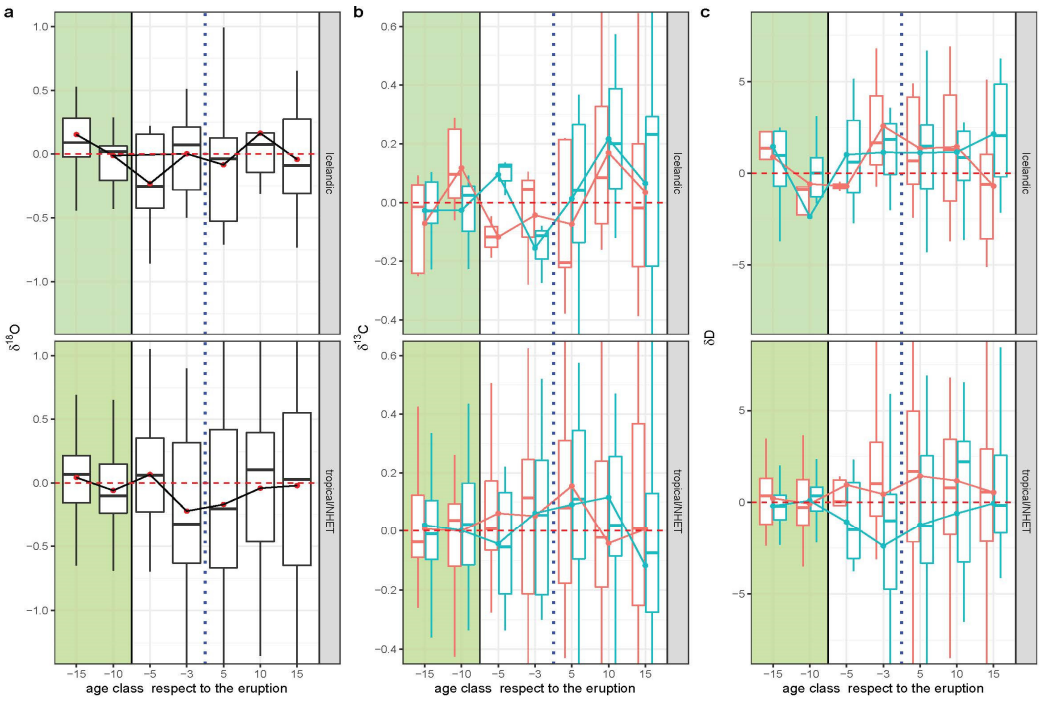

Figure 8. Analysis of the main volcanic eruptions after 0 CE: Boxplots of the cellulose isotope anomaly ($\delta^{18}O$ (**a**); $\delta^{13}C$ (**b**); δD (**c**)) for the 34 strongest volcanic eruptions after 0 CE included in [2]. The cellulose isotope values are from the Eastern Alpine Conifer Chronology database and have a 5-year resolution. The Northern Hemisphere Extra Tropical (NHET) and tropical eruptions are separated from the Icelandic ones; the larch trees and the cembran pine are represented as red and blue boxes, respectively. The data are aligned on the year of the eruption, indicated by the blue dotted vertical line. Forcing and response are calculated to a 10-year background period before the eruption, with the assumption that it is undisturbed by volcanic eruptions. The solid lines connect the mean value of each boxplot. The calibration period is shaded in green, and the horizontal red dotted line is the average of the calibration period. The points are the mean values of each boxplot.

3.1.4. Isotopes' Climatic Sensitivity in the Recent Period

A correlation analysis of the climatic variables and the EACC data may provide information on the climate sensitivity of each cellulose isotope. We averaged the isotope data of different samples for the same years from all sites; we considered the larch and cembran pine species separately and together and compared them to climate variables (i.e., summer temperature, summer precipitation, and sunshine) (Supplementary Figure S2). We then calculated the correlations of isotope series with the summer (June, July, August) temperature and precipitation time series from 1850 CE to 1980 CE. For the sunshine duration, we used the data from 1880 to 1980 CE available from the HISTALP database [68]. We chose these periods because we selected samples with a cambial age > 100 years to avoid age effects [67].

Additionally, we chose to avoid the recent past (after 1980), in which isotope values diverged from climate variables due to the recent climate [72]. In fact, after 1980 the isotopes of the two species present different trends, even in the same region; the oxygen isotope value increased in larch, while it remained unchanged in cembran pine larch (Figure S2). This difference is unprecedented in the past 200 years, but the scarcity of data prevents us from investigating it more in detail.

To avoid geographical effects [67], we normalised each tree instead of using the "raw data" and averaged all values. Figure 9a–c show that the $\delta^{18}O$ of both species has a significant negative correlation with precipitation (r value of about −0.5) but a positive correlation with temperature and sunshine. The $\delta^{13}C$ of cembran pine is significantly positively correlated with temperature, while that of larch has no significant correlation

with temperature, precipitation, or sunshine. Deuterium has no significant correlation with temperature, precipitation, or sunshine in either species. The oxygen isotope is the only isotope with similar climatic correlation between the two species, while carbon and hydrogen show different or even opposite climatic correlations in the two species. The precipitation and temperature of JJA are correlated, with an r value of −0.5.

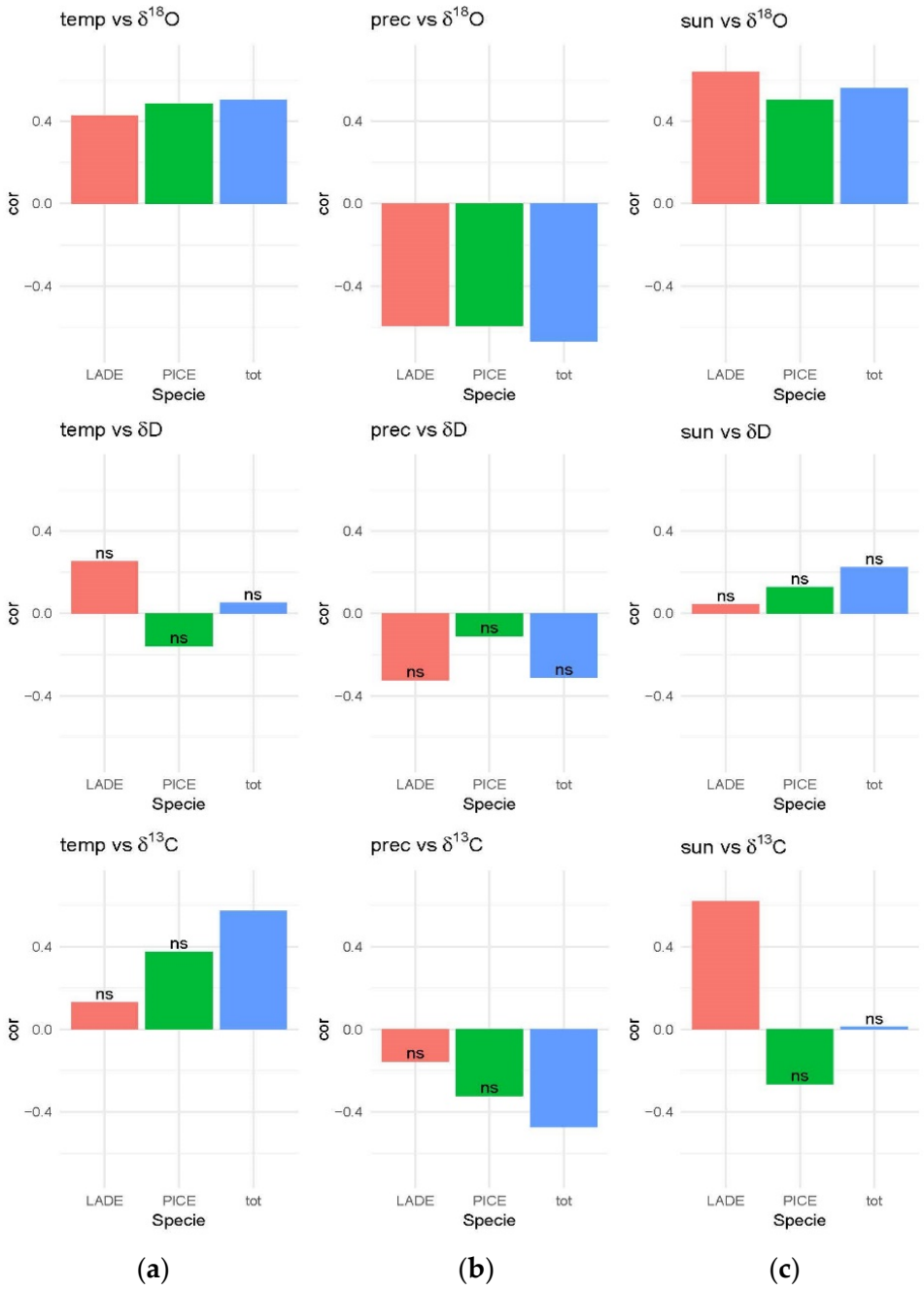

Figure 9. Climate correlations of cellulose isotopes: Pearson's correlation coefficient between the mean of 5 years of (**a**) temperature anomaly, (**b**) precipitation anomaly, and (**c**) mean sunshine duration from the HISTALP database [68] with cellulose isotopes with 5-year time resolution; for oxygen, the two species were merged (blue) in the larch (LADE, orange) and cembran pine (PICE, green). The data are from 1880 to 1970 CE for temperature and precipitation, and from 1880 to 1970 CE for mean sunshine duration; ns: non-significant.

4. Discussion

Large volcanic eruptions in the tropics and extratropics can perturb the climate system, peaking for 1–3 years [73], but climate responses depend critically on the eruptions' source parameters, such as the strength of radiative forcing, the location, the and season of the eruption. Here, we explored how large volcanic eruptions in the tropics and from Iceland affected the stable isotopes' variability in an array of temperature-sensitive tree-ring records from the European Alps (the AHTTRIR database) over the past 2000 years. This database seems to be well-suited for this study, since models project that the climate at the sampling sites (in the Alps between 45° and 47° northern latitude) is strongly influenced by both tropical and Icelandic eruptions, e.g., [3,74]. Moreover, observations, along with climate and glacier reconstructions, show a strong sensitivity of the alpine climate to volcanic forcing (e.g., [5,75,76]). We compared the isotopic values of tree-ring cellulose with proxies for the European climate and direct temperature measurements, as well as with the reconstructed temperatures based on the hydrogen isotope ratios of speleothem fluid inclusions from Milandre Cave in Switzerland [42], which provided information on the cold seasons not accessible from the tree-ring records.

We first analysed the well-documented eruption of the tropical volcano Tambora in 1815 CE, which was followed by a "year without a summer" in some parts of Europe [5]. The results show that the $\delta^{18}O$ values varied after the eruption, with good agreement between the data of larch and cembran pine and those of 1-year and 5-year resolution. Thus, the $\delta^{18}O$ data are of sufficient robustness for climatic investigation, in agreement with [28], and represent a better climate proxy than the other cellulose isotopes [77]. In fact, the δD and $\delta^{13}C$ values showed no consistent variations in the years around the eruption. To further assess the robustness of $\delta^{18}O$ climate signals, we compared them with the summer temperature, precipitation, and sunshine duration of that period derived from the HISTALP database [68]. The decrease in the $\delta^{18}O$ signal between 1809 and 1815 is consistent with the HISTALP summer temperature variability, and also with the temperature reconstructions based on MXD data [70] and TRW [69]. They all also show the influence of an unidentified volcanic eruption in 1809, which caused a cooling phase in Europe [35]. However, this is not evident in the annual temperature of the Swiss Plateau, suggesting difference in season sensitivity. The cellulose is synthesised in the growing season (summer), and its $\delta^{18}O$ mainly reflects summer temperatures and precipitation, while the Swiss Plateau reflects the annual temperature through the fluid inclusion. The speleothem data show a clear minimal temperature centred around 1810 CE [42], which would indicate that both the summer and the winter temperatures in Switzerland cooled after those eruptions. Thus, the comparison between the different proxy data should yield seasonal climate information. The cellulose $\delta^{18}O$ recovered rapidly after the Tambora eruption, similar to MDX and to the measured temperatures, while TRW-derived temperatures showed a longer recovery time. This suggests the absence of biological memory in cellulose $\delta^{18}O$ (as in MDX) that is present in TRW [27]. The minimum cellulose $\delta^{18}O$ value coincided with the 1815 CE eruption, while the minimum of the other proxies was one year later. A similar one-year lag between the eruption and the tree rings' proxy response was already reported for Siberian larch [31]. It is worth noting that the isotopes of Central European oak and the $\delta^{18}O$ of Siberian larch at high- and low-altitude sites were not affected by the Tambora eruption [31,69]. In fact, the most anomalous cold summer temperatures were reported in Switzerland and eastern France, with a well-documented increase in summer precipitations over Southern–Central Europe in 1816 [9], while Russia and Ukraine reported only a milder summer [5]. We found that the cellulose $\delta^{18}O$ had a positive relationship with temperature and a negative relationship with precipitation, so the strong negative peak could be the sum of the two effects.

We also conducted a detailed analysis of the mid-8th-century period (720–780 CE), when a cluster of possibly Icelandic eruptions occurred. The data showed a good agreement between the $\delta^{18}O$ values of larch and cembran pine and between the 1-year- and 5-year-resolved data. Such an agreement was not observed for $\delta^{13}C$. However, all of the iso-

topes showed constant variability throughout the whole period, without evident changes around the eruptions. There are no direct temperature measurements in this ancient epoch that could be used for comparison. Nevertheless, summer temperature reconstructions are available from MDX and TRW data [69,70]. These show only minor changes in this period, likely explained by the smaller magnitudes of sulphur injection into the atmosphere by the eruption. The reconstructed temperatures provided good correlations with the mean cellulose $\delta^{18}O$ at annual resolution. The 750s–760s eruptions were mainly reported to cause winter cooling, and one European historical source describes the 763/64 winter as among the most outstanding cold episodes of the last 2000 years [78]. The speleothem data show decreases in temperature values centred around 730 and 790 CE, albeit with significant age uncertainties. The analysis of the Tambora and Iceland eruptions presented above indicated that even the 5-year-resolution data of the EACC database provide information on climatic changes caused by the eruptions. We therefore used this database to study the periods of two other well-characterised eruptions—of the Icelandic volcano Laki in 1783 CE, and of the tropical volcano Samalas in 1257 CE. We found evident signals of cellulose $\delta^{18}O$ and δD that occurred around the date of the Laki eruption and that showed a pattern similar to that of the temperature reconstruction from TRW [69]. Moreover, the positive $\delta^{18}O$ peak fits with the very high summer temperature experienced in Western Europe in 1783, followed by a very cold winter [79]. The long-lasting fissure eruption of Laki in 1783–1784, emitting over 100 Tg of SO_2 into the atmosphere, likely had a different forcing potential and climate footprint than the assumed but otherwise poorly characterised prehistoric Icelandic eruptions of Katla, Grímsvötn, and Bárdarbunga in the mid-8th century.

The Laki eruption caused cold winter temperatures and a warm and dry summer in Europe [80,81], explaining the positive peak in TRW $\delta^{18}O$ and δD. A similar analysis of Central European oaks at low altitudes gave the opposite results, i.e., no signal after the Laki and tropical eruptions, but a negative Palmer Drought Severity Index for the Icelandic eruptions [33]. Around the period of the 1257 Samalas eruption, only the cellulose $\delta^{18}O$ of larch showed minimal values. A temperature change was detected only in the reconstruction from MXD. The Samalas eruption of 1257 was reported to have affected the European hydroclimate, with a 3-year cooling and an increase in summer precipitation in Southern Europe but a decrease in Northern Europe [10]. Nothing significant could be seen from the speleothem record.

We analysed the 5-year binned cellulose isotope values of the database around 34 strong volcanic eruptions over the last 2000 years, as listed in Table S1 [2]. The results showed lower mean $\delta^{18}O$ values near the eruptions that persisted for up to 10 years after the events, in agreement with previous analyses of the volcanic impact on climate reconstructed from TRW data [2,69]. Similar analyses have been conducted previously—Siberian larches showed lower post-eruption $\delta^{18}O$ values and $\delta^{13}C$ values for three different sites [31]. In Scandinavian pine trees at northern latitudes, $\delta^{13}C$ values have lower post-eruption values, likely related to changes in solar irradiance [30]. In our case, a climate relationship of $\delta^{13}C$ with sunshine was also observed, but only for the larch. The $\delta^{13}C$ values of larch and cembran pine showed a lower value around the Icelandic eruptions, followed by value increments, while after the "NHET + Tropical" eruptions an increase was visible in both species.

The δD trends were different for larch and cembran pine in the "NHET + Tropical" eruptions, probably due to their different biological isotopic fractionation [67]. In larch the values slightly increased, while in cembran pine the values were lower, with a pattern similar to that of oxygen. This difference may be attributed to the strong post-eruption cooling that caused lower δD values of precipitation, which was more represented in the cembran pine than in the larch. In a previous work, we found that larch showed a higher correlation between oxygen and hydrogen isotope data than cembran pine [82]. We attributed the strongest signal in the cellulose $\delta^{18}O$ to the impact of both temperature and precipitation, since the tropical eruptions not only have a cooling effect but also produce circulation feedbacks at a continental scale that cause distinct effects on regional

precipitation patterns [9]. In the superposed analysis of 34 eruptions, the speleothem fluid inclusion temperature record could not be included due to its low temporal resolution.

5. Conclusions

In conclusion, our data show that the $\delta^{18}O$ values of cellulose in the larches and cembran pines show patterns similar to those of the meteorological parameters, recording the very strong eruptions of Tambora, Laki, and Samalas, but not the lower sulphur-emitting eruptions in the mid-8th century. The $\delta^{18}O$ of cellulose was more sensitive to the tropical eruptions than to the Icelandic ones, probably because the tropical eruptions had a larger cooling effect on the alpine summer climate and increased summer precipitation in Southern Europe. Cellulose $\delta^{18}O$ shows no memory effect after an eruption, similarly to MDX, making it an excellent proxy for studying short-term climate variability. The $\delta^{13}C$ and δD values showed no consistent signals, possibly because the sample replication of the database was too low. Their marginal or non-significant correlations suggest that these values of the two conifers species should be treated separately. The analysis of superimposed major eruptions over the past 2000 years confirms the importance of the oxygen data, which clearly show lower values around the tropical/NHET eruptions while lacking a clear common signal around the Icelandic eruptions. The significance of carbon and deuterium isotopes remains unclear.

Altogether, the isotope data with 5-year resolution from the AHTTRIR database provide climate signals of eruptions, but the data with annual resolution are more informative and, if used in a multiproxy approach, can resolve seasonal climate signals, as shown in this publication for the Tambora eruption.

Supplementary Materials: The following supporting information can be downloaded at: https://www.mdpi.com/article/10.3390/geosciences12100371/s1, Table S1: Parameter for the 34 volcanic eruptions; Figure S1: (a) Spatially and temporally resolved Stratospheric Aerosol Optical Depth (SAOD) reconstruction based on ice cores between 1804–1826 with volcanic eruptions in 1809 and 1815 (Toohey & Sigl 2017). (b) Spatially and temporally resolved SAOD reconstruction based on ice cores between CE 748-768 with volcanic eruptions in CE 750, 756 and 764 (Toohey & Sigl 2017); Figure S2: Timeline used for the correlation of Figure 8. The values are shown in z-score to be compared in red the values of larch, green the value of cembran pine and blue the mean values in the three isorope. In black the values of the climatic variable (a) temperature, (b) precipitation, (c) sunshine. The correlation of Figure 8 considers the time window from 1850 to 1980 for precipitation and temperature. For sunshine was use the time windows 1870–1980.

Author Contributions: T.A. and M.M.Z.-W. performed the cellulose stable-isotope analyses. R.S. and E.S. performed the cellulose stable-isotope analyses of the two annual-resolution trees. T.A. drafted the first version of the manuscript. K.N. and C.S. were responsible for collecting, analysing, and crossdating the wood material. M.C.L., K.N., M.S. and S.A. contributed to the evaluation of the results. M.C.L., K.N., M.S. and S.A. conceived of the presented idea. All authors have read and agreed to the published version of the manuscript.

Funding: This research was supported by the Swiss National Science Foundation (SNF 200021L_144255, SNF 200020_172550) as well as by the Austrian Science Fund (FWF, grant I-265 1183-N19) and the Oeschger Centre for Climate Change Research, University of Bern, Bern, Switzerland (OCCR). This study was part of the "STALCLIM" and "STALCLIM 2" Sinergia projects funded by the Swiss National Science Foundation (grant nos. CRSI22-132646 and CRSII2_147674). This research has been also supported by the European Research Council Horizon 2020 Research and Innovation program (THERA; grant no. 820047).

Institutional Review Board Statement: Not applicable.

Informed Consent Statement: Not applicable.

Data Availability Statement: The tree-rings isotope dataset is available to the public after the official completion of the Alpine Holocene Tree-Ring Isotope Records (AHTRIR) project: https://doi.pangaea.de/10.1594/PANGAEA.941604. The tree-ring isotope data with an annual resolution can be obtained

upon request. Speleothem fluid inclusion water isotopes and inferred temperatures from Milandre Cave, Switzerland, are available to the public: https://doi.org/10.1594/PANGAEA.904949.

Acknowledgments: We are grateful to Peter Nyfeler for the precious assistance during stable isotope measurements, to Andrea Thurner and Andreas Österreicher for the preparation of the isotope samples from Alpine sites, and to the civil service collaborators Lars Herrmann, Giacomo Ruggia, Jonathan Lamprecht, Yannick Rohrer, Rafael Zuber, Andrea Weibel, and Rafael Ottersberg.

Conflicts of Interest: The authors declare no conflict of interest.

References

1. Robock, A. Volcanic Eruptions and Climate. *Rev. Geophys.* **2000**, *38*, 191–219. [CrossRef]
2. Sigl, M.; Winstrup, M.; McConnell, J.R.; Welten, K.C.; Plunkett, G.; Ludlow, F.; Büntgen, U.; Caffee, M.; Chellman, N.; Dahl-Jensen, D. Timing and Climate Forcing of Volcanic Eruptions for the Past 2500 Years. *Nature* **2015**, *523*, 543–549. [CrossRef] [PubMed]
3. Oman, L.; Robock, A.; Stenchikov, G.; Schmidt, G.A.; Ruedy, R. Climatic Response to High-Latitude Volcanic Eruptions. *J. Geophys. Res. Atmos.* **2005**, *110*, D13103. [CrossRef]
4. Toohey, M.; Krüger, K.; Schmidt, H.; Timmreck, C.; Sigl, M.; Stoffel, M.; Wilson, R. Disproportionately Strong Climate Forcing from Extratropical Explosive Volcanic Eruptions. *Nat. Geosci.* **2019**, *12*, 100–107. [CrossRef]
5. Raible, C.C.; Brönnimann, S.; Auchmann, R.; Brohan, P.; Frölicher, T.L.; Graf, H.-F.; Jones, P.; Luterbacher, J.; Muthers, S.; Neukom, R. Tambora 1815 as a Test Case for High Impact Volcanic Eruptions: Earth System Effects. *Wiley Interdiscip. Rev. Clim. Chang.* **2016**, *7*, 569–589. [CrossRef] [PubMed]
6. Schaller, N.; Griesser, T.; Fischer, A.; STICK-LER, A.; Onnimann, S. Climate Effects of the 1883 Krakatoa Eruption: Historical and Present Perspectives. *Vjschr. Natf. Ges. Zürich* **2009**, *154*, 31–40.
7. Zambri, B.; Robock, A.; Mills, M.J.; Schmidt, A. Modeling the 1783–1784 Laki Eruption in Iceland: 2. Climate Impacts. *J. Geophys. Res. Atmos.* **2019**, *124*, 6770–6790. [CrossRef]
8. Edwards, J. The Enigmatic Northwestern North American Climate Response to the 1783 Laki Eruption. Ph.D. Thesis, The University of Arizona, Tucson, AZ, USA, 2020.
9. Wegmann, M.; Brönnimann, S.; Bhend, J.; Franke, J.; Folini, D.; Wild, M.; Luterbacher, J. Volcanic Influence on European Summer Precipitation through Monsoons: Possible Cause for "Years without Summer". *J. Clim.* **2014**, *27*, 3683–3691. [CrossRef]
10. Liu, B.; Liu, J.; Ning, L.; Sun, W.; Yan, M.; Zhao, C.; Chen, K.; Wang, X. The Role of Samalas Mega Volcanic Eruption in European Summer Hydroclimate Change. *Atmosphere* **2020**, *11*, 1182. [CrossRef]
11. Esper, J.; Schneider, L.; Krusic, P.J.; Luterbacher, J.; Büntgen, U.; Timonen, M.; Sirocko, F.; Zorita, E. European Summer Temperature Response to Annually Dated Volcanic Eruptions over the Past Nine Centuries. *Bull. Volcanol.* **2013**, *75*, 736. [CrossRef]
12. Luterbacher, J.; Werner, J.P.; Smerdon, J.E.; Fernández-Donado, L.; González-Rouco, F.J.; Barriopedro, D.; Ljungqvist, F.C.; Büntgen, U.; Zorita, E.; Wagner, S. European Summer Temperatures since Roman Times. *Environ. Res. Lett.* **2016**, *11*, 024001. [CrossRef]
13. Stoffel, M.; Khodri, M.; Corona, C.; Guillet, S.; Poulain, V.; Bekki, S.; Guiot, J.; Luckman, B.H.; Oppenheimer, C.; Lebas, N. Estimates of Volcanic-Induced Cooling in the Northern Hemisphere over the Past 1500 Years. *Nat. Geosci.* **2015**, *8*, 784–788. [CrossRef]
14. D'Arrigo, R.; Wilson, R.; Tudhope, A. The Impact of Volcanic Forcing on Tropical Temperatures during the Past Four Centuries. *Nat. Geosci.* **2009**, *2*, 51–56. [CrossRef]
15. Rao, M.P.; Cook, B.I.; Cook, E.R.; D'Arrigo, R.D.; Krusic, P.J.; Anchukaitis, K.J.; LeGrande, A.N.; Buckley, B.M.; Davi, N.K.; Leland, C. European and Mediterranean Hydroclimate Responses to Tropical Volcanic Forcing over the Last Millennium. *Geophys. Res. Lett.* **2017**, *44*, 5104–5112. [CrossRef] [PubMed]
16. Fritz, H. *Tree Rings: Basics and Applications of Dendrochronology*; Springer Science & Business Media: Dordrecht, The Netherlands, 1976.
17. Büntgen, U.; Wacker, L.; Galvan, J.; Arnold, S.; Arseneault, D.; Baillie, M.; Beer, J.; Bernabei, M.; Bleicher, N.; Boswijk, G. Tree Rings Reveal Globally Coherent Signature of Cosmogenic Radiocarbon Events in 774 and 993 CE. *Nat. Commun.* **2018**, *9*, 3605. [CrossRef] [PubMed]
18. PAGES2k. A Global Multiproxy Database for Temperature Reconstructions of the Common Era. *Sci. Data* **2017**, *4*, 170088. [CrossRef]
19. Reinig, F.; Wacker, L.; Jöris, O.; Oppenheimer, C.; Guidobaldi, G.; Nievergelt, D.; Adolphi, F.; Cherubini, P.; Engels, S.; Esper, J. Precise Date for the Laacher See Eruption Synchronizes the Younger Dryas. *Nature* **2021**, *595*, 66–69. [CrossRef] [PubMed]
20. Büntgen, U.; Eggertsson, Ó.; Wacker, L.; Sigl, M.; Ljungqvist, F.C.; Di Cosmo, N.; Plunkett, G.; Krusic, P.J.; Newfield, T.P.; Esper, J. Multi-Proxy Dating of Iceland's Major Pre-Settlement Katla Eruption to 822–823 CE. *Geology* **2017**, *45*, 783–786. [CrossRef]
21. Oppenheimer, C.; Wacker, L.; Xu, J.; Galván, J.D.; Stoffel, M.; Guillet, S.; Corona, C.; Sigl, M.; Di Cosmo, N.; Hajdas, I. Multi-Proxy Dating the 'Millennium Eruption'of Changbaishan to Late 946 CE. *Quat. Sci. Rev.* **2017**, *158*, 164–171. [CrossRef]
22. Anchukaitis, K.J.; Breitenmoser, P.; Briffa, K.R.; Buchwal, A.; Büntgen, U.; Cook, E.R.; D'arrigo, R.D.; Esper, J.; Evans, M.N.; Frank, D. Tree Rings and Volcanic Cooling. *Nat. Geosci.* **2012**, *5*, 836–837. [CrossRef]
23. Büntgen, U.; Kolář, T.; Rybníček, M.; Koňasová, E.; Trnka, M.; Ač, A.; Krusic, P.J.; Esper, J.; Treydte, K.; Reinig, F.; et al. No Age Trends in Oak Stable Isotopes. *Paleoceanogr. Paleoclimatology* **2020**, *35*. [CrossRef]
24. Altman, J.; Saurer, M.; Dolezal, J.; Maredova, N.; Song, J.-S.; Ho, C.-H.; Treydte, K. Large Volcanic Eruptions Reduce Landfalling Tropical Cyclone Activity: Evidence from Tree Rings. *Sci. Total Environ.* **2021**, *775*, 145899. [CrossRef]

25. Esper, J.; Konter, O.; Krusic, P.J.; Saurer, M.; Holzkämper, S.; Büntgen, U. Long-Term Summer Temperature Variations in the Pyrenees from Detrended Stable Carbon Isotopes. *Geochronometria* **2015**, *42*, 53–59. [CrossRef]
26. Lücke, L.J.; Hegerl, G.C.; Schurer, A.P.; Wilson, R. Effects of Memory Biases on Variability of Temperature Reconstructions. *J. Clim.* **2019**, *32*, 8713–8731. [CrossRef]
27. Esper, J.; Schneider, L.; Smerdon, J.E.; Schöne, B.R.; Büntgen, U. Signals and Memory in Tree-Ring Width and Density Data. *Dendrochronologia* **2015**, *35*, 62–70. [CrossRef]
28. McCarroll, D.; Loader, N.J. Stable Isotopes in Tree Rings. *Quat. Sci. Rev.* **2004**, *23*, 771–801. [CrossRef]
29. Churakova, O.V.; Bryukhanova, M.V.; Saurer, M.; Boettger, T.; Naurzbaev, M.M.; Myglan, V.S.; Vaganov, E.A.; Hughes, M.K.; Siegwolf, R.T. A Cluster of Stratospheric Volcanic Eruptions in the AD 530s Recorded in Siberian Tree Rings. *Glob. Planet. Chang.* **2014**, *122*, 140–150. [CrossRef]
30. Helama, S.; Arppe, L.; Uusitalo, J.; Holopainen, J.; Mäkelä, H.M.; Mäkinen, H.; Mielikäinen, K.; Nöjd, P.; Sutinen, R.; Taavitsainen, J.-P. Volcanic Dust Veils from Sixth Century Tree-Ring Isotopes Linked to Reduced Irradiance, Primary Production and Human Health. *Sci. Rep.* **2018**, *8*, 1339. [CrossRef]
31. Sidorova, O.V.; Saurer, M.; Guillet, S.; Corona, C.; Fonti, P.; Myglan, V.S.; Kirdyanov, A.V.; Naumova, O.V.; Ovchinnikov, D.V.; Shashkin, A.V. Siberian Tree-Ring and Stable Isotope Proxies as Indicators of Temperature and Moisture Changes after Major Stratospheric Volcanic Eruptions. *Clim. Past* **2019**, *15*, 685–700.
32. Battipaglia, G.; Cherubini, P.; Saurer, M.; Siegwolf, R.T.; Strumia, S.; Francesca Cotrufo, M. Volcanic Explosive Eruptions of the Vesuvio Decrease Tree-Ring Growth but Not Photosynthetic Rates in the Surrounding Forests. *Glob. Chang. Biol.* **2007**, *13*, 1122–1137. [CrossRef]
33. Büntgen, U.; Urban, O.; Krusic, P.J.; Rybníček, M.; Kolář, T.; Kyncl, T.; Ač, A.; Koňasová, E.; Čáslavskỳ, J.; Esper, J. Recent European Drought Extremes beyond Common Era Background Variability. *Nat. Geosci.* **2021**, *14*, 190–196. [CrossRef]
34. Büntgen, U.; Allen, K.; Anchukaitis, K.J.; Arseneault, D.; Boucher, É.; Bräuning, A.; Chatterjee, S.; Cherubini, P.; Churakova, O.V.; Corona, C. The Influence of Decision-Making in Tree Ring-Based Climate Reconstructions. *Nat. Commun.* **2021**, *12*, 3411. [CrossRef] [PubMed]
35. Kress, A.; Saurer, M.; Siegwolf, R.T.; Frank, D.C.; Esper, J.; Bugmann, H. A 350 Year Drought Reconstruction from Alpine Tree Ring Stable Isotopes. *Glob. Biogeochem. Cycles* **2010**, *24*, 2. [CrossRef]
36. Grießinger, J.; Bräuning, A.; Helle, G.; Schleser, G.H.; Hochreuther, P.; Meier, W.J.-H.; Zhu, H. A Dual Stable Isotope Approach Unravels Common Climate Signals and Species-Specific Responses to Environmental Change Stored in Multi-Century Tree-Ring Series from the Tibetan Plateau. *Geosciences* **2019**, *9*, 151. [CrossRef]
37. Reynolds-Henne, C.E.; Siegwolf, R.T.W.; Treydte, K.S.; Esper, J.; Henne, S.; Saurer, M. Temporal Stability of Climate-Isotope Relationships in Tree Rings of Oak and Pine (Ticino, Switzerland). *Glob. Biogeochem. Cycles* **2007**, *21*, 4. [CrossRef]
38. Gagen, M.; McCarroll, D.; Edouard, J.-L. Combining Ring Width, Density and Stable Carbon Isotope Proxies to Enhance the Climate Signal in Tree-Rings: An Example from the Southern French Alps. *Clim. Chang.* **2006**, *78*, 363–379. [CrossRef]
39. Treydte, K.; Schleser, G.H.; Schweingruber, F.H.; Winiger, M. The Climatic Significance of δ 13 C in Subalpine Spruces (Lötschental, Swiss Alps): A Case Study with Respect to Altitude, Exposure and Soil Moisture. *Tellus B Chem. Phys. Meteorol.* **2001**, *53*, 593–611. [CrossRef]
40. Vitali, V.; Martínez-Sancho, E.; Treydte, K.; Andreu-Hayles, L.; Dorado-Liñán, I.; Gutierrez, E.; Helle, G.; Leuenberger, M.; Loader, N.J.; Rinne-Garmston, K.T. The Unknown Third–Hydrogen Isotopes in Tree-Ring Cellulose across Europe. *Sci. Total Environ.* **2022**, *813*, 152281. [CrossRef]
41. Wieloch, T.; Grabner, M.; Augusti, A.; Serk, H.; Ehlers, I.; Yu, J.; Schleucher, J. Metabolism Is the Major Driver of Hydrogen Isotope Fractionation Recorded in Tree-Ring Glucose of Pinus Nigra. *N. Phytol.* **2021**, *234*, 449–461. [CrossRef]
42. Affolter, S.; Häuselmann, A.; Fleitmann, D.; Edwards, R.L.; Cheng, H.; Leuenberger, M. Central Europe Temperature Constrained by Speleothem Fluid Inclusion Water Isotopes over the Past 14,000 Years. *Sci. Adv.* **2019**, *5*, eaav3809. [CrossRef] [PubMed]
43. Nicolussi, K.; Kaufmann, M.; Melvin, T.M.; Van Der Plicht, J.; Schießling, P.; Thurner, A. A 9111 Year Long Conifer Tree-Ring Chronology for the European Alps: A Base for Environmental and Climatic Investigations. *Holocene* **2009**, *19*, 909–920. [CrossRef]
44. Arosio, T.; Ziehmer, M.; Nicolussi, K.; Schluechter, C.; Thurner, A.; Österreicher, A.; Nyfeler, P.; Leuenberger, M.C. *Alpine Holocene Triple Tree Ring Isotope Record*; PANGAEA Publishing: Bremen, Germany, 2022. [CrossRef]
45. Arosio, T.; Ziehmer, M.M.; Nicolussi, K.; Schlüchter, C.; Leuenberger, M. Alpine Holocene Tree-Ring Dataset: Age-Related Trends in the Stable Isotopes of Cellulose Show Species-Specific Patterns. *Biogeosciences* **2020**, *17*, 4871–4882. [CrossRef]
46. Ziehmer, M.M.; Nicolussi, K.; Schlüchter, C.; Leuenberger, M. Preliminary Evaluation of the Potential of Tree-Ring Cellulose Content as a Novel Supplementary Proxy in Dendroclimatology. *Biogeosciences* **2018**, *15*, 1047–1064. [CrossRef]
47. Loader, N.J.; Street-Perrott, F.A.; Daley, T.J.; Hughes, P.D.M.; Kimak, A.; Levanic, T.; Mallon, G.; Mauquoy, D.; Robertson, I.; Roland, T.P. Simultaneous Determination of Stable Carbon, Oxygen, and Hydrogen Isotopes in Cellulose. *Anal. Chem.* **2015**, *87*, 376–380. [CrossRef]
48. Filot, M.S.; Leuenberger, M.; Pazdur, A.; Boettger, T. Rapid Online Equilibration Method to Determine the D/H Ratios of Non-Exchangeable Hydrogen in Cellulose. *Rapid Commun. Mass Spectrom.* **2006**, *20*, 3337–3344. [CrossRef]
49. Coplen, T.B. Reporting of Stable Hydrogen, Carbon, and Oxygen Isotopic Abundances (Technical Report). *Pure Appl. Chem.* **1994**, *66*, 273–276. [CrossRef]
50. Leuenberger, M. To What Extent Can Ice Core Data Contribute to the Understanding of Plant Ecological Developments of the Past. *Terr. Ecol.* **2007**, *1*, 211–233.

51. Suess, H.E. Radiocarbon Concentration in Modern Wood. *Science* **1955**, *122*, 415–417. [CrossRef]
52. Cole-Dai, J.; Ferris, D.; Lanciki, A.; Savarino, J.; Baroni, M.; Thiemens, M.H. Cold Decade (AD 1810–1819) Caused by Tambora (1815) and Another (1809) Stratospheric Volcanic Eruption. *Geophys. Res. Lett.* **2009**, *36*, 22. [CrossRef]
53. Timmreck, C.; Toohey, M.; Zanchettin, D.; Brönnimann, S.; Lundstadt, E.; Wilson, R. The Unidentified Volcanic Eruption of 1809: Why It Remains a Climatic Cold Case. *Clim. Past Discuss.* **2021**, 1–39.
54. Oppenheimer, C. Climatic, Environmental and Human Consequences of the Largest Known Historic Eruption: Tambora Volcano (Indonesia) 1815. *Prog. Phys. Geogr.* **2003**, *27*, 230–259. [CrossRef]
55. Lavigne, F.; Degeai, J.-P.; Komorowski, J.-C.; Guillet, S.; Robert, V.; Lahitte, P.; Oppenheimer, C.; Stoffel, M.; Vidal, C.M. Surono Source of the Great AD 1257 Mystery Eruption Unveiled, Samalas Volcano, Rinjani Volcanic Complex, Indonesia. *Proc. Natl. Acad. Sci. USA* **2013**, *110*, 16742–16747. [CrossRef]
56. Vidal, C.M.; Métrich, N.; Komorowski, J.-C.; Pratomo, I.; Michel, A.; Kartadinata, N.; Robert, V.; Lavigne, F. The 1257 Samalas Eruption (Lombok, Indonesia): The Single Greatest Stratospheric Gas Release of the Common Era. *Sci. Rep.* **2016**, *6*, 34868. [CrossRef] [PubMed]
57. Büntgen, U.; Smith, S.H.; Wagner, S.; Krusic, P.; Esper, J.; Piermattei, A.; Crivellaro, A.; Reinig, F.; Tegel, W.; Kirdyanov, A. Global Tree-Ring Response and Inferred Climate Variation Following the Mid-Thirteenth Century Samalas Eruption. *Clim. Dyn.* **2022**, *59*, 531–546. [CrossRef]
58. Guillet, S.; Corona, C.; Stoffel, M.; Khodri, M.; Lavigne, F.; Ortega, P.; Eckert, N.; Sielenou, P.D.; Daux, V.; Davi, N. Climate Response to the Samalas Volcanic Eruption in 1257 Revealed by Proxy Records. *Nat. Geosci.* **2017**, *10*, 123–128. [CrossRef]
59. Thordarson, T.; Self, S. Atmospheric and Environmental Effects of the 1783–1784 Laki Eruption: A Review and Reassessment. *J. Geophys. Res. Atmos.* **2003**, *108*, AAC-7. [CrossRef]
60. Dawson, A.G.; Kirkbride, M.P.; Cole, H. Atmospheric Effects in Scotland of the AD 1783–1784 Laki Eruption in Iceland. *Holocene* **2021**, *31*, 830–843. [CrossRef]
61. Elíasson, J. Katla Volcano in Iceland, Potential Hazards and Risk Assessment. *Nat. Sci.* **2014**, *6*, 9. [CrossRef]
62. Gudmundsdottir, E.R.; Larsen, G.; Eiriksson, J. Tephra Stratigraphy on the N Orth I Celandic Shelf: Extending Tephrochronology into Marine Sediments off N Orth I Celand. *Boreas* **2012**, *41*, 719–734. [CrossRef]
63. Óladóttir, B.A.; Sigmarsson, O.; Larsen, G. Tephra Productivity and Eruption Flux of the Subglacial Katla Volcano, Iceland. *Bull. Volcanol.* **2018**, *80*, 58. [CrossRef]
64. Óladóttir, B.A.; Larsen, G.; Sigmarsson, O. Volume Estimates of Nine Katla Tephra Layers (1860 BC–870 AD). *Jökull* **2014**, *64*, 23–40.
65. Óladóttir, B.A.; Sigmarsson, O.; Larsen, G.; Thordarson, T. Katla Volcano, Iceland: Magma Composition, Dynamics and Eruption Frequency as Recorded by Holocene Tephra Layers. *Bull. Volcanol.* **2008**, *70*, 475–493. [CrossRef]
66. Toohey, M.; Sigl, M. Volcanic Stratospheric Sulfur Injections and Aerosol Optical Depth from 500 BCE to 1900 CE. *Earth Syst. Sci. Data* **2017**, *9*, 809–831. [CrossRef]
67. Arosio, T.; Ziehmer-Wenz, M.M.; Nicolussi, K.; Schlüchter, C.; Leuenberger, M. Larch Cellulose Shows Significantly Depleted Hydrogen Isotope Values With Respect to Evergreen Conifers in Contrast to Oxygen and Carbon Isotopes. *Front. Earth Sci.* **2020**, *8*, 579. [CrossRef]
68. Auer, I.; Böhm, R.; Jurkovic, A.; Lipa, W.; Orlik, A.; Potzmann, R.; Schöner, W.; Ungersböck, M.; Matulla, C.; Briffa, K. HISTALP—Historical Instrumental Climatological Surface Time Series of the Greater Alpine Region. *Int. J. Climatol. A J. R. Meteorol. Soc.* **2007**, *27*, 17–46. [CrossRef]
69. Büntgen, U.; Tegel, W.; Nicolussi, K.; McCormick, M.; Frank, D.; Trouet, V.; Kaplan, J.O.; Herzig, F.; Heussner, K.-U.; Wanner, H. 2500 Years of European Climate Variability and Human Susceptibility. *Science* **2011**, *331*, 578–582. [CrossRef]
70. Büntgen, U.; Frank, D.C.; Nievergelt, D.; Esper, J. Summer Temperature Variations in the European Alps, AD 755–2004. *J. Clim.* **2006**, *19*, 5606–5623. [CrossRef]
71. Pfister, C.; Rohr, C. Euro-Climhist. BORIS. 2015. Available online: https://boris.unibe.ch/id/eprint/73058 (accessed on 4 August 2022).
72. Savard, M.M.; Daux, V. An Overview on Isotopic Divergences–Causes for Instability of Tree-Ring Isotopes and Climate Correlations. *Clim. Past* **2020**, *16*, 1223–1243. [CrossRef]
73. Cole-Dai, J. Volcanoes and Climate. *Wiley Interdiscip. Rev. Clim. Chang.* **2010**, *1*, 824–839. [CrossRef]
74. Brönnimann, S.; Franke, J.; Nussbaumer, S.U.; Zumbühl, H.J.; Steiner, D.; Trachsel, M.; Hegerl, G.C.; Schurer, A.; Worni, M.; Malik, A. Last Phase of the Little Ice Age Forced by Volcanic Eruptions. *Nat. Geosci.* **2019**, *12*, 650–656. [CrossRef]
75. Büntgen, U.; Myglan, V.S.; Ljungqvist, F.C.; McCormick, M.; Di Cosmo, N.; Sigl, M.; Jungclaus, J.; Wagner, S.; Krusic, P.J.; Esper, J. Cooling and Societal Change during the Late Antique Little Ice Age from 536 to around 660 AD. *Nat. Geosci.* **2016**, *9*, 231–236. [CrossRef]
76. Sigl, M.; Abram, N.J.; Gabrieli, J.; Jenk, T.M.; Osmont, D.; Schwikowski, M. 19th Century Glacier Retreat in the Alps Preceded the Emergence of Industrial Black Carbon Deposition on High-Alpine Glaciers. *Cryosphere* **2018**, *12*, 3311–3331. [CrossRef]
77. Klesse, S.; Weigt, R.; Treydte, K.; Saurer, M.; Schmid, L.; Siegwolf, R.T.; Frank, D.C. Oxygen Isotopes in Tree Rings Are Less Sensitive to Changes in Tree Size and Relative Canopy Position than Carbon Isotopes. *Plant Cell Environ.* **2018**, *41*, 2899–2914. [CrossRef] [PubMed]
78. McCormick, M.; Dutton, P.E.; Mayewski, P.A. Volcanoes and the Climate Forcing of Carolingian Europe, AD 750–950. *Speculum* **2007**, *82*, 865–895. [CrossRef]
79. Schmidt, A.; Thordarson, T.; Oman, L.D.; Robock, A.; Self, S. Climatic Impact of the Long-Lasting 1783 Laki Eruption: Inapplicability of Mass-Independent Sulfur Isotopic Composition Measurements. *J. Geophys. Res. Atmos.* **2012**, *117*, D23. [CrossRef]

80. Edwards, J.; Anchukaitis, K.J.; Gunnarson, B.E.; Pearson, C.; Seftigen, K.; von Arx, G.; Linderholm, H.W. The Origin of Tree-Ring Reconstructed Summer Cooling in Northern Europe During the 18th Century Eruption of Laki. *Paleoceanogr. Paleoclimatology* **2022**, *37*, e2021PA004386. [CrossRef]
81. Salvador, I.; Romano, M.; Avanzini, M. Gli "Apparenti Disordini Delle Leggi Fisiche Dell'universo": Gli Effetti Delle Eruzioni Del Laki (1783) e Del Tambora (1815) Nelle Cronache Delle Regioni Alpine. *Tre Secoli Di Geol. Ital. Rend. Online Della Soc. Geol. Ital.* **2018**, *44*, 72–79. [CrossRef]
82. Arosio, T.; Ziehmer-Wenz, M.M.; Nicolussi, K.; Schlüchter, C.; Leuenberger, M.C. Investigating Masking Effects of Age Trends on the Correlations among Tree Ring Proxies. *Forests* **2021**, *12*, 1523. [CrossRef]